Isogeometric Buckling Analysis of The Magneto-electro-elastic Foam Plates Resting on An Elastic Foundation

P. T. HUNG[1,*], *P. PHUNG-VAN*[2]

[1]Faculty of Civil Engineering, Ho Chi Minh City University of Technology and Education, Ho Chi Minh City, Vietnam
[2]Faculty of Civil Engineering, HUTECH University, Ho Chi Minh City, Vietnam

*Corresponding Author: P. T. HUNG (Email: hungpht@hcmute.edu.vn)
(Received: 13-Feb-2023; accepted: 13-Mar-2023; published: 31-Mar-2023)
DOI: http://dx.doi.org/10.55579/jaec.202371.398

Abstract. *This study combines the isogeometric approach (IGA) and refined plate theory (RPT) with two variables to investigate the buckling behavior of magneto-electro-elastic (MEE) foam plates resting on an elastic foundation. The pores in the MEE foam plates are arranged in three patterns: uniform, symmetric, and asymmetric distributions across the plate thickness. The elastic foundation supported by Winkler and Pasternak is utilized to approach the computational model. The governing equations are derived by using RPT and Hamilton's principle. The Non-Uniform Rational B-Splines (NURBS) basic functions in the IGA method are used to approximate the displacement fields and magnetic and electric potentials. The critical buckling load of the MEE foam plates is determined by solving the above governing equations with the help of the IGA. The study investigates and discusses the influence of various parameters such as porosity distributions, porous coefficient, external electric voltage and magnetic potential, spring/shear coefficients of the elastic foundation, and the geometry of the MEE foam plates on the critical buckling load. The results show that these parameters significantly influence the buckling behavior of the MEE foam plates. This study provides valuable insights into the buckling behavior of magneto-electro-elastic foam plates and can inform the design of novel materials and structures with tailored properties.*

Keywords

Magneto-electro-elastic foam plate, isogeometric analysis, buckling analysis, refined plate theory, elastic foundations.

1. Introduction

A magneto-electro-elastic material is a type of material that has both magnetic and electro-elastic behavior. This material can be used in various applications, including vibration damping, sensing, and energy harvesting. It is unique because it combines magnetic and electric fields with mechanical deformation to produce a composite behavior tailored to specific needs. The mechanical, electrical, and magnetic properties of the material can be controlled and optimized through the design and fabrication process, making it a promising candidate for a wide range of technological applications. Therefore, numerous investigations have been into the mechanical behaviors of the MEE structures in recent years. Ramirez et al. [1] studied the free vibration of the laminated plates with homogeneous elastic, piezoelectric and piezomagnetic layers. Employing the semi-analytical finite element method, Xin et al. [2, 3] presented the free vibration analysis of the fixed supported and simply supported multilayer MEE plates. Li and Zhang [4] used the Mindlin theory and analytical method to investigate the free vibration of the MEE plate resting on an elastic foundation. Besides, according to the third-order beam theory and nonlocal elasticity theory, the analytical thermal buckling of the magneto-electro-thermo-elastic (METE) functionally graded (FG) nanobeams was examined by Ebrahimi et al. [5]. Liu [6] presented the bending of the laminated plates with MEE layers using the Kirchhoff plate theory (KPT) and the analytical method. The KPT and modified strain gradient theory are used by Jamalpoor et al. [7] to investigate the analytical size-dependent buckling and free vibration of the MEE microplate resting on a visco-Pasternak foundation considering the external electric and magnetic loads. Moreover, Ansari and Gholami [8] studied the buckling and post-buckling analyses of the METE nanoplates under external mechanical, magnetic, electric and thermal loads employing the nonlocal elasticity theory and nonlinear first-order plate theory. Shooshtari et al. [9] found the analytical natural frequency of the rectangular MEE plates resting on an elastic foundation based on the higher-order shear deformation theory (HSDT). According to the HSDT and analytical method, Razavi [10] presented the mechanical buckling of the MEE plates with axial and biaxial compressive loads. The analytical buckling of the MEE nanoplates according to the nonlocal elastic theory and the HSDT was investigated by Park et al. [11]. Malikan et al. [12] used the simple FSDT combined with nonlocal strain gradient theory to present the forced vibration of the MEE nanoplates based on the analytical method. The nonlinear bending of the MEE plates with linear variable thickness was studied by Wang et al. [13] based on von Karman plate theory. Yang et al. [14] investigated the influence of the surface effect on the analytical free vibration and bending of the circular MEE nanoplates under the external electric voltage and magnetic potential employing the KPT. Based on the nonlocal elasticity theory, Arefi et al. [15] present the bending and buckling of the three-layered doubly curved nanoshells with homogeneous core and MEE face sheets according to the analytical method. Based on the third-order shear deformation theory, Hong et al. [16] studied the analytical vibration of FG cylindrical shell in a thermal environment. Solby et al. [17], employing the refined shear deformation theory, studied the free vibration of the MEE FG plate reinforced by the graphene platelets resting on an elastic substrate.

As we see in the above literature review, the MEE structure was studied by using the analytical method, which is suitable for a simple problem with a simple boundary. The numerical method, such as finite element method (FEM), meshfree, IGA, etc., are the best choice for the problem with complex boundaries. In addition, Kiran and Kattimani [18, 19] used FSDT and the finite element method (FEM) to find the critical buckling load of the multilayered rectangular and skew plates with piezoelectric and piezomagnetic layers. The IGA can efficiently fulfill the higher-order derivatives of the refined plate theory due to its foundation in Non-uniform rational B-splines (NURBS) basic functions, which provide versatility in achieving any preferred level of continuity within the basis functions. The IGA and its computational expense is first proposed by Hughes [20]. Bazilevs et al. [21] analyzed the wind turbines and turbomachinery using IGA. Furthermore, according to IGA, microplate size-dependent free vibration, bending, and buckling can be examined in references [22, 23, 24]. The free vibration and static analyses of the FGM plate and the buckling of the Mindlin–Reissner plates were introduced in [25, 26] employing the extended IGA. Tajikawa et al. [27] investigated computational cardiovascular medicine based on the IGA. Based on the isogeometric mesh-free collocation method, the free vibration, static bending and mechanical buckling of the laminated composite plates were investigated by Huang et al. [28]. Zhang et al. [29] proposed the nonlocal operator method for solving complex multifield problems. Besides, Zhou et al. [30] provided an optimal solution to address the problem of reducing the degree of C-Bézier surfaces with prescribed constraints in the L2 norm. According to the isogeometric-reproducing kernel particle method, Kiran et al. [31] presented the buckling of the orthotropic three-dimensional plates and shells containing cracks.

As far as the authors know that there has not been a study that uses IGA and RPT with two variables to examine the buckling of the MEE foam plate resting on the Winkler-Pasternak foundation. This article fills that research gap by using RPT with two variables and IGA to perform the mechanical buckling of the MEE foam plates resting on a Winkler-Pasternak foundation. The impact of the porous distribution types, porosity coefficient, external electric and magnetic loads, shear and spring coefficients of the elastic foundation and geometric parameters on the MEE foam plates is analyzed and discussed.

2. The Basic Equations

2.1. The MEE foam plates

As we see in Figure 1, the MEE foam plate with porosities is arranged in uniform, symmetric, and asymmetric distributions across the plate thickness, respectively. The effective material properties of the MEE foam plate are presented as follows [32]

Uniform:

$$\begin{cases} P_{eff} = P_1\left(1 - e_0\xi\right) \\ \rho_{eff} = \rho_1\left(1 - e_m\xi\right) \\ \xi = \frac{1}{e_0} - \frac{1}{e_0}\left(\frac{2}{\pi}\sqrt{1-e_0} - \frac{2}{\pi} + 1\right)^2 \end{cases}$$

Symmetric:

$$\begin{cases} P_{eff} = P_1\left(1 - e_0\cos\left(\frac{\pi z}{h}\right)\right) \\ \rho_{eff} = \rho_1\left(1 - e_m\cos\left(\frac{\pi z}{h}\right)\right) \end{cases} \tag{1}$$

Asymmetric:

$$\begin{cases} P_{eff} = P_1\left(1 - e_0\cos\left(\frac{\pi z}{2h} + \frac{\pi}{4}\right)\right) \\ \rho_{eff} = \rho_1\left(1 - e_m\cos\left(\frac{\pi z}{2h} + \frac{\pi}{4}\right)\right) \end{cases}$$

where

$$\begin{cases} e_0 = 1 - \dfrac{E_2}{E_1} = 1 - \dfrac{G_2}{G_1}, 0 < e_0 < 1 \\ e_m = 1 - \dfrac{\rho_2}{\rho_1}; 0 < e_m < 1 \end{cases} \tag{2}$$

in which P and ρ are the material properties and density of the MEE foam plates, respectively; e_0 is the porous coefficient, e_m is the porosity coefficient of density; E and G are the moduli of elasticity and shear modulus, respectively. Indexes "1" and "2" indicate the maximum and minimum values of the material properties, respectively.

2.2. The refined plate theory with two variables

The vector of displacement fields at any point in the MEE foam plate is represented by using the RPT [33] as follows

$$\mathbf{u} = \begin{Bmatrix} u \\ v \\ w \end{Bmatrix} = \mathbf{u}_1 + z\mathbf{u}_2 + f\left(z\right)\mathbf{u}_3 = ...$$
$$\begin{Bmatrix} 0 \\ 0 \\ w_b + w_s \end{Bmatrix} + z\begin{Bmatrix} -w_{b,x} \\ -w_{b,y} \\ 0 \end{Bmatrix} + f\left(z\right)\begin{Bmatrix} w_{s,x} \\ w_{s,y} \\ 0 \end{Bmatrix} \tag{3}$$

in which w_b and w_s represent the bending and shear transverse displacements along the z-axis, respectively; symbol "," describes the differential operator; $f(z)$ represents the distribution function, which is specified as

$$f\left(z\right) = -\frac{4z^3}{3h^2} \tag{4}$$

Based on Eq. (3), the linear strain tensor components are defined by

$$\begin{cases} \varepsilon_x = -zw_{b,xx} + f\left(z\right)w_{s,xx} \\ \varepsilon_y = -zw_{b,yy} + f\left(z\right)w_{s,yy} \\ \gamma_{xy} = -2zw_{b,xy} + 2f\left(z\right)w_{s,xy} \\ \gamma_{xz} = \left(1 + f'\left(z\right)\right)w_{s,x} \\ \gamma_{yz} = \left(1 + f'\left(z\right)\right)w_{s,y} \end{cases} \tag{5}$$

Eq. (5) is rewritten in matrix form as follows

$$\boldsymbol{\varepsilon} = \begin{Bmatrix} \boldsymbol{\varepsilon}_b \\ \boldsymbol{\varepsilon}_s \end{Bmatrix} = \begin{Bmatrix} z\boldsymbol{\varepsilon}_{b1} + f\left(z\right)\boldsymbol{\varepsilon}_{b2} \\ \left(1 + f'\left(z\right)\right)\boldsymbol{\gamma}_s \end{Bmatrix} \tag{6}$$

where

$$\boldsymbol{\varepsilon}_b = \begin{Bmatrix} \varepsilon_x \\ \varepsilon_y \\ \gamma_{xy} \end{Bmatrix}; \boldsymbol{\varepsilon}_{b1} = -\begin{Bmatrix} w_{b,xx} \\ w_{b,yy} \\ 2w_{b,xy} \end{Bmatrix}; \boldsymbol{\varepsilon}_{b2} = \begin{Bmatrix} w_{s,xx} \\ w_{s,yy} \\ 2w_{s,xy} \end{Bmatrix};$$
$$\boldsymbol{\varepsilon}_s = \begin{Bmatrix} \gamma_{xz} \\ \gamma_{yz} \end{Bmatrix}; \boldsymbol{\gamma}_s = \begin{Bmatrix} w_{s,x} \\ w_{s,y} \end{Bmatrix} \tag{7}$$

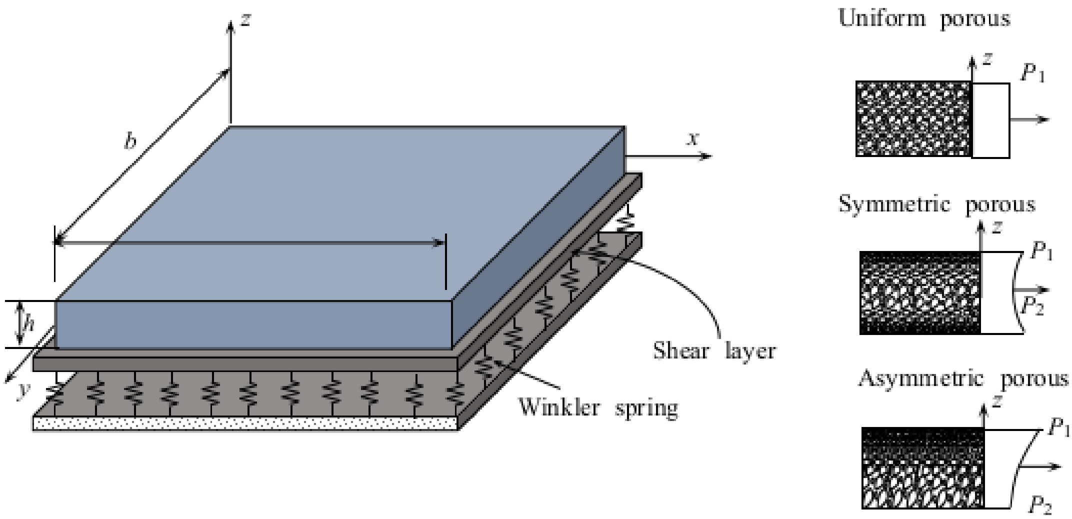

Fig. 1: The geometry of the MEE foam plates resting on an elastic foundation.

In accordance with Maxwell's equation, as outlined in [34], the electric and magnetic potentials can be taken by the following forms

$$\begin{cases} \Phi\left(x,y,z\right)=g\left(z\right)\varphi\left(x,y\right)+\dfrac{2z}{h}V_0; \\ \Psi\left(x,y,z\right)=g\left(z\right)\psi\left(x,y\right)+\dfrac{2z}{h}\Omega_0 \end{cases} \tag{8}$$

where $g\left(z\right)=-\cos\left(\pi z/h\right)$; Φ and Ψ are the electric and magnetic potentials, respectively; V_0 and Ω_0 are the initial external electric voltage and magnetic potential, respectively.

The electric and magnetic fields are obtained from the electric and magnetic potentials according to Eq. (8) as follows

$$\begin{aligned} \mathbf{E}&=\begin{Bmatrix} E_x \\ E_y \\ E_z \end{Bmatrix}=-\begin{Bmatrix} \Phi_{,x} \\ \Phi_{,y} \\ \Phi_{,z} \end{Bmatrix}=-\begin{Bmatrix} g\left(z\right)\varphi_{,x} \\ g\left(z\right)\varphi_{,x} \\ g'\left(z\right)\varphi+\frac{2V_0}{h} \end{Bmatrix}; \\ \mathbf{H}&=\begin{Bmatrix} H_x \\ H_y \\ H_z \end{Bmatrix}=-\begin{Bmatrix} \Psi_{,x} \\ \Psi_{,y} \\ \Psi_{,z} \end{Bmatrix}=-\begin{Bmatrix} g\left(z\right)\psi_{,x} \\ g\left(z\right)\psi_{,x} \\ g'\left(z\right)\psi+\frac{2\Omega_0}{h} \end{Bmatrix} \end{aligned} \tag{9}$$

in which E_x, E_y, E_z are the electric field's components and H_x, H_y, H_z are the magnetic field's components.

2.3. Constitutive equations

The constitutive relations of the MEE foam plate are formulated as follows [7]

$$\begin{aligned} &\begin{Bmatrix} \sigma_x \\ \sigma_y \\ \tau_{xy} \\ \tau_{xz} \\ \tau_{yz} \end{Bmatrix}=\begin{bmatrix} \bar{c}_{11} & \bar{c}_{12} & 0 & 0 & 0 \\ \bar{c}_{12} & \bar{c}_{22} & 0 & 0 & 0 \\ 0 & 0 & \bar{c}_{66} & 0 & 0 \\ 0 & 0 & 0 & \bar{c}_{44} & 0 \\ 0 & 0 & 0 & 0 & \bar{c}_{55} \end{bmatrix}\begin{Bmatrix} \varepsilon_x \\ \varepsilon_y \\ \gamma_{xy} \\ \gamma_{xz} \\ \gamma_{yz} \end{Bmatrix}-... \\ &\begin{bmatrix} 0 & 0 & \bar{e}_{31} \\ 0 & 0 & \bar{e}_{31} \\ 0 & 0 & 0 \\ \bar{e}_{15} & 0 & 0 \\ 0 & \bar{e}_{15} & 0 \end{bmatrix}\begin{Bmatrix} E_x \\ E_y \\ E_z \end{Bmatrix}-\begin{bmatrix} 0 & 0 & \bar{q}_{31} \\ 0 & 0 & \bar{q}_{31} \\ 0 & 0 & 0 \\ \bar{q}_{15} & 0 & 0 \\ 0 & \bar{q}_{15} & 0 \end{bmatrix}\begin{Bmatrix} H_x \\ H_y \\ H_z \end{Bmatrix}; \\ &\begin{Bmatrix} D_x \\ D_y \\ D_z \end{Bmatrix}=\begin{Bmatrix} 0 & 0 & 0 & \bar{e}_{15} & 0 \\ 0 & 0 & 0 & 0 & \bar{e}_{15} \\ \bar{e}_{31} & \bar{e}_{31} & 0 & 0 & 0 \end{Bmatrix}\begin{Bmatrix} \varepsilon_x \\ \varepsilon_y \\ \gamma_{xy} \\ \gamma_{xz} \\ \gamma_{yz} \end{Bmatrix}+... \\ &\begin{bmatrix} \bar{k}_{11} & 0 & 0 \\ 0 & \bar{k}_{22} & 0 \\ 0 & 0 & \bar{k}_{33} \end{bmatrix}\begin{Bmatrix} E_x \\ E_y \\ E_z \end{Bmatrix}+\begin{bmatrix} \bar{d}_{11} & 0 & 0 \\ 0 & \bar{d}_{22} & 0 \\ 0 & 0 & \bar{d}_{33} \end{bmatrix}\begin{Bmatrix} H_x \\ H_y \\ H_z \end{Bmatrix}; \\ &\begin{Bmatrix} B_x \\ B_y \\ B_z \end{Bmatrix}=\begin{Bmatrix} 0 & 0 & 0 & \bar{q}_{15} & 0 \\ 0 & 0 & 0 & 0 & \bar{q}_{15} \\ \bar{q}_{31} & \bar{q}_{31} & 0 & 0 & 0 \end{Bmatrix}\begin{Bmatrix} \varepsilon_x \\ \varepsilon_y \\ \gamma_{xy} \\ \gamma_{xz} \\ \gamma_{yz} \end{Bmatrix}+... \\ &\begin{bmatrix} \bar{d}_{11} & 0 & 0 \\ 0 & \bar{d}_{22} & 0 \\ 0 & 0 & \bar{d}_{33} \end{bmatrix}\begin{Bmatrix} E_x \\ E_y \\ E_z \end{Bmatrix}+\begin{bmatrix} \bar{\mu}_{11} & 0 & 0 \\ 0 & \bar{\mu}_{22} & 0 \\ 0 & 0 & \bar{\mu}_{33} \end{bmatrix}\begin{Bmatrix} H_x \\ H_y \\ H_z \end{Bmatrix} \end{aligned} \tag{10}$$

where $\sigma_x, \sigma_y, \tau_{xy}, \tau_{xz}$ and τ_{yz} are the stress tensor's components; D_x, D_y, D_z and H_x, H_y, H_z are electric and magnetic displacements, respectively; $\bar{c}_{ij}$ is the reduced elastic stiffness's components; $\bar{e}_{ij}$, $\bar{q}_{ij}$ and $\bar{k}_{ij}$ are the reduced piezo-electric, piezo-magnetic and dielectric permittivity, respectively; $\bar{d}_{ij}$ and $\bar{\mu}_{ij}$ are reduced electro-magnetic and magnetic permittivity coefficients, respectively. The reduced material properties in Eq. (10) are formulated as follows

$$\begin{aligned}
&\bar{c}_{11} = c_{11} - \frac{c_{13}^2}{c_{33}};\ \bar{c}_{12} = c_{12} - \frac{c_{13}^2}{c_{33}};\\
&\bar{c}_{66} = c_{66};\ \bar{c}_{55} = c_{55};\ \bar{c}_{44} = c_{44};\\
&\bar{e}_{31} = e_{31} - \frac{e_{33}c_{13}}{c_{33}};\ \bar{e}_{15} = e_{15};\\
&\bar{q}_{31} = q_{31} - \frac{q_{33}c_{13}}{c_{33}};\ \bar{q}_{15} = q_{15};\\
&\bar{k}_{33} = k_{33} + \frac{e_{33}^2}{c_{33}};\ \bar{k}_{11} = k_{11};\\
&\bar{d}_{33} = d_{33} + \frac{q_{33}e_{33}}{c_{33}};\ \bar{d}_{11} = d_{11};\\
&\bar{\mu}_{33} = \mu_{33} + \frac{q_{33}^2}{c_{33}};\ \bar{\mu}_{11} = \mu_{11}
\end{aligned} \tag{11}$$

where the coefficients c_{ij}, e_{ij}, q_{ij}, k_{ij}, d_{ij}, μ_{ij} are calculated from Eq. (1). In matrix form, the constitutive equations (10) are reformed by

$$\begin{cases}
\boldsymbol{\sigma}_b = \mathbf{C}_{uub}\boldsymbol{\varepsilon}_b - \mathbf{C}_{ueb}\mathbf{E}_b - \boldsymbol{C}_{umb}\boldsymbol{H}_b;\\
\boldsymbol{\sigma}_s = \mathbf{C}_{uus}\boldsymbol{\varepsilon}_s - \mathbf{C}_{ues}\mathbf{E}_s - \mathbf{C}_{ums}\boldsymbol{H}_s;\\
\mathbf{D}_b = \mathbf{C}_{ueb}^T\boldsymbol{\varepsilon}_b + \mathbf{C}_{eeb}\mathbf{E}_b + \mathbf{C}_{emb}\boldsymbol{H}_b;\\
\mathbf{D}_s = \mathbf{C}_{ues}^T\boldsymbol{\varepsilon}_s + \mathbf{C}_{ees}\mathbf{E}_s + \mathbf{C}_{ems}\boldsymbol{H}_s;\\
\mathbf{B}_b = \mathbf{C}_{umb}^T\boldsymbol{\varepsilon}_b + \mathbf{C}_{emb}\mathbf{E}_b + \mathbf{C}_{mmb}\boldsymbol{H}_b;\\
\mathbf{B}_s = \mathbf{C}_{ums}^T\boldsymbol{\varepsilon}_s + \mathbf{C}_{ems}\mathbf{E}_s + \mathbf{C}_{mms}\boldsymbol{H}_s
\end{cases} \tag{12}$$

where

$$\begin{aligned}
&\boldsymbol{\sigma}_b = \begin{Bmatrix}\sigma_x & \sigma_y & \tau_{xy}\end{Bmatrix}^T;\ \boldsymbol{\sigma}_s = \begin{Bmatrix}\tau_{xz} & \tau_{yz}\end{Bmatrix}^T;\\
&\mathbf{D}_b = \begin{Bmatrix}0 & 0 & D_z\end{Bmatrix}^T;\ \mathbf{D}_s = \begin{Bmatrix}D_x & D_y\end{Bmatrix}^T;\\
&\mathbf{B}_b = \begin{Bmatrix}0 & 0 & B_z\end{Bmatrix}^T;\ \mathbf{B}_s = \begin{Bmatrix}B_x & B_y\end{Bmatrix}^T;\\
&\mathbf{E}_b = \begin{Bmatrix}0 & 0 & E_z\end{Bmatrix}^T;\mathbf{E}_s = \begin{Bmatrix}E_x & E_y\end{Bmatrix}^T;\\
&\mathbf{H}_b = \begin{Bmatrix}0 & 0 & H_z\end{Bmatrix}^T;\mathbf{H}_s = \begin{Bmatrix}H_x & H_y\end{Bmatrix}^T
\end{aligned} \tag{13}$$

and

$$\begin{aligned}
&\mathbf{C}_{uub} = \begin{bmatrix}\bar{c}_{11} & \bar{c}_{12} & 0\\ \bar{c}_{12} & \bar{c}_{22} & 0\\ 0 & 0 & \bar{c}_{66}\end{bmatrix};\ \mathbf{C}_{ueb} = \begin{bmatrix}0 & 0 & \bar{e}_{31}\\ 0 & 0 & \bar{e}_{31}\\ 0 & 0 & 0\end{bmatrix};\\
&\mathbf{C}_{umb} = \begin{bmatrix}0 & 0 & \bar{q}_{31}\\ 0 & 0 & \bar{q}_{31}\\ 0 & 0 & 0\end{bmatrix};\ \mathbf{C}_{eeb} = \begin{bmatrix}0 & 0 & 0\\ 0 & 0 & 0\\ 0 & 0 & \bar{k}_{33}\end{bmatrix};\\
&\mathbf{C}_{mmb} = \begin{bmatrix}0 & 0 & 0\\ 0 & 0 & 0\\ 0 & 0 & \bar{\mu}_{33}\end{bmatrix};\ \mathbf{C}_{emb} = \begin{bmatrix}0 & 0 & 0\\ 0 & 0 & 0\\ 0 & 0 & \bar{d}_{33}\end{bmatrix};\\
&\mathbf{C}_{uus} = \begin{bmatrix}\bar{c}_{44} & 0\\ 0 & \bar{c}_{55}\end{bmatrix};\ \mathbf{C}_{ues} = \begin{bmatrix}\bar{e}_{15} & 0\\ 0 & \bar{e}_{15}\end{bmatrix};\\
&\mathbf{C}_{ums} = \begin{bmatrix}\bar{q}_{15} & 0\\ 0 & \bar{q}_{15}\end{bmatrix};\ \mathbf{C}_{ees} = \begin{bmatrix}\bar{k}_{11} & 0\\ 0 & \bar{k}_{11}\end{bmatrix};\\
&\mathbf{C}_{mms} = \begin{bmatrix}\bar{\mu}_{11} & 0\\ 0 & \bar{\mu}_{22}\end{bmatrix};\ \mathbf{C}_{ems} = \begin{bmatrix}\bar{d}_{11} & 0\\ 0 & \bar{d}_{22}\end{bmatrix}
\end{aligned} \tag{14}$$

2.4. Variational principle

Based on Hamilton's principle, the governing equation for the mechanical buckling of an MEE foam plate resting on an elastic foundation can be expressed as

$$\int_0^t (\delta\Pi - \delta V_{em} - \delta V_f - \delta V_m)\,\mathrm{d}t = 0 \tag{15}$$

where $\delta\Pi$ represents the virtual strain energy, δV_{em} is the virtual work done by the external electric voltage and magnetic potential, δV_f is the virtual work done by an elastic foundation, δV_m is the virtual work done by the external compressive loads.

The virtual strain energy of the MEE foam plate is expressed as

$$\delta\Pi = \int_V \begin{pmatrix}\delta\boldsymbol{\varepsilon}_b^T\boldsymbol{\sigma}_b + \delta\boldsymbol{\varepsilon}_s^T\boldsymbol{\sigma}_s - \delta\mathbf{E}_b^T\mathbf{D}_b - ...\\ \delta\mathbf{E}_s^T\mathbf{D}_s - \delta\mathbf{H}_b^T\mathbf{B}_b - \delta\mathbf{H}_s^T\mathbf{B}_s\end{pmatrix} dV \tag{16}$$

The virtual work performed by the initial external electric and magnetic loads is formulated by

$$\delta V_{em} = \int_{\Omega} \delta \mathbf{N}_w^T \mathbf{N}_{em} \mathbf{N}_w \mathrm{d}\Omega; \quad \mathbf{N}_{em} = -\begin{bmatrix} 2\bar{e}_{31}V_0 + 2\bar{q}_{31}\Omega_0 & 0 \\ 0 & 2\bar{e}_{31}V_0 + 2\bar{q}_{31}\Omega_0 \end{bmatrix}; \quad \mathbf{N}_w = \begin{Bmatrix} w_{b,x} + w_{s,x} \\ w_{b,y} + w_{s,y} \end{Bmatrix} \tag{17}$$

The virtual work performed by the Winkler-Pasternak foundation is expressed as

$$\delta V_f = \int_{\Omega} \delta \mathbf{N}_w^T \left(k_w \mathbf{N}_w - k_s \nabla^2 \mathbf{N}_w \right) \mathrm{d}\Omega \tag{18}$$

where $\nabla = \frac{\partial}{\partial x} + \frac{\partial}{\partial y}$ is the gradient operator; k_w and k_s are spring and shear coefficients of the Winkler-Pasternak foundation, respectively.

In addition, the virtual work done by the external compressive loads can be expressed by

$$\delta V_m = \int_{\Omega} \delta \mathbf{N}_w^T \mathbf{N}_m \mathbf{N}_w \mathrm{d}\Omega; \ \mathbf{N}_m = \begin{bmatrix} N_x & 0 \\ 0 & N_y \end{bmatrix} \tag{19}$$

where N_x and N_y are the inplane external compressive loads.

By substituting the appropriate expressions into Eq. (15), the weak form of the governing equation can be rewritten as following

$$\begin{aligned}
&\int_{\Omega} \delta\left(\bar{\varepsilon}^b\right)^T \bar{\boldsymbol{D}}_{uub} \bar{\varepsilon}^b \mathrm{d}\Omega - \int_{\Omega} \delta\left(\bar{\varepsilon}^b\right)^T \bar{\boldsymbol{D}}_{ueb} \bar{\mathbf{E}}^b \mathrm{d}\Omega - ... \\
&\int_{\Omega} \delta\left(\bar{\varepsilon}^b\right)^T \bar{\boldsymbol{D}}_{umb} \bar{\mathbf{H}}^b \mathrm{d}\Omega + \int_{\Omega} \delta(\boldsymbol{\gamma}^s)^T \bar{\boldsymbol{D}}_{uus} \boldsymbol{\gamma}^s \mathrm{d}\Omega - ... \\
&\int_{\Omega} \delta(\boldsymbol{\gamma}^s)^T \bar{\boldsymbol{D}}_{ues} \bar{\mathbf{E}}^s \mathrm{d}\Omega - \int_{\Omega} \delta(\boldsymbol{\gamma}^s)^T \bar{\boldsymbol{D}}_{ums} \bar{\mathbf{H}}^s \mathrm{d}\Omega - ... \\
&\int_{\Omega} \delta\left(\bar{\mathbf{E}}^b\right)^T \bar{\boldsymbol{D}}_{ueb}^T \bar{\varepsilon}^b \mathrm{d}\Omega - \int_{\Omega} \delta\left(\bar{\mathbf{E}}^b\right)^T \bar{\boldsymbol{D}}_{eeb} \bar{\mathbf{E}}^b \mathrm{d}\Omega - ... \\
&\int_{\Omega} \delta\left(\bar{\mathbf{E}}^b\right)^T \bar{\boldsymbol{D}}_{emb} \bar{\mathbf{H}}^b \mathrm{d}\Omega - \int_{\Omega} \delta\left(\bar{\mathbf{E}}^s\right)^T \bar{\boldsymbol{D}}_{ues}^T \boldsymbol{\gamma}^s \mathrm{d}\Omega - ... \\
&\int_{\Omega} \delta\left(\bar{\mathbf{E}}^s\right)^T \bar{\boldsymbol{D}}_{ees} \bar{\mathbf{E}}^s \mathrm{d}\Omega - \int_{\Omega} \delta\left(\bar{\mathbf{E}}^s\right)^T \bar{\boldsymbol{D}}_{ems} \bar{\mathbf{H}}^s \mathrm{d}\Omega - ... \\
&\int_{\Omega} \delta\left(\bar{\mathbf{H}}^b\right)^T \bar{\boldsymbol{D}}_{umb}^T \bar{\varepsilon}^b \mathrm{d}\Omega - \int_{\Omega} \delta\left(\bar{\mathbf{H}}^b\right)^T \bar{\boldsymbol{D}}_{emb} \bar{\mathbf{E}}^b \mathrm{d}\Omega - ... \\
&\int_{\Omega} \delta\left(\bar{\mathbf{H}}^b\right)^T \bar{\boldsymbol{D}}_{mmb} \bar{\mathbf{H}}^b \mathrm{d}\Omega - \int_{\Omega} \delta\left(\bar{\mathbf{H}}^s\right)^T \bar{\boldsymbol{D}}_{ums}^T \gamma^s \mathrm{d}\Omega - ... \\
&\int_{\Omega} \delta\left(\bar{\mathbf{H}}^s\right)^T \bar{\boldsymbol{D}}_{ems} \bar{\mathbf{E}}^s \mathrm{d}\Omega - \int_{\Omega} \delta\left(\bar{\mathbf{H}}^s\right)^T \bar{\boldsymbol{D}}_{mms} \bar{\mathbf{H}}^s \mathrm{d}\Omega - ... \\
&\int_{\Omega} \delta \mathbf{N}_w^T \mathbf{N}_{em} \mathbf{N}_w \mathrm{d}\Omega = \int_{\Omega} \delta \mathbf{N}_w^T \mathbf{N}_m \mathbf{N}_w \mathrm{d}\Omega + ... \\
&\int_{\Omega} \delta \mathbf{N}_w^T \left(k_w \mathbf{N}_w - k_s \nabla^2 \mathbf{N}_w \right) \mathrm{d}\Omega
\end{aligned} \tag{20}$$

where

$$\begin{aligned}
&\bar{\varepsilon}^b = \begin{Bmatrix} \varepsilon_{b1} \\ \varepsilon_{b2} \end{Bmatrix}; \bar{\mathbf{E}}^b = -\begin{Bmatrix} 0 & 0 & \varphi \end{Bmatrix}^T; \bar{\mathbf{E}}^s = -\begin{Bmatrix} \varphi_{,x} & \varphi_{,y} \end{Bmatrix}^T; \\
&\bar{\mathbf{H}}^b = -\begin{Bmatrix} 0 & 0 & \psi \end{Bmatrix}^T; \bar{\mathbf{H}}^s = -\begin{Bmatrix} \psi_{,x} & \psi_{,y} \end{Bmatrix}^T; \\
&\bar{\boldsymbol{D}}_{uub} = \begin{bmatrix} \boldsymbol{A}_b & \boldsymbol{B}_b \\ \boldsymbol{B}_b & \boldsymbol{D}_b \end{bmatrix}; \bar{\boldsymbol{D}}_{uus} = \int_{-h/2}^{h/2} (1+f')^2 \mathbf{C}_{uus} \mathrm{d}z; \\
&(\boldsymbol{A}_b, \boldsymbol{B}_b, \boldsymbol{D}_b) = \int_{-h/2}^{h/2} \left(z^2, zf, f^2\right) \mathbf{C}_{uub} \mathrm{d}z; \\
&\bar{\boldsymbol{D}}_{ueb} = \left\{ \mathbf{C}_{ueb}^1 \quad \mathbf{C}_{ueb}^2 \right\}; \bar{\boldsymbol{D}}_{umb} = \left\{ \mathbf{C}_{umb}^1 \quad \mathbf{C}_{umb}^2 \right\}; \\
&\left(\mathbf{C}_{ueb}^1, \mathbf{C}_{ueb}^2\right) = \int_{-h/2}^{h/2} \mathbf{C}_{ueb} \left(z, f\right) g' \mathrm{d}z; \\
&\left(\mathbf{C}_{umb}^1, \mathbf{C}_{umb}^2\right) = \int_{-h/2}^{h/2} \mathbf{C}_{umb} \left(z, f\right) g' \mathrm{d}z; \\
&\bar{\mathbf{D}}_{ues} = \int_{-h/2}^{h/2} \mathbf{C}_{ues} \left(1+f'\right) g \mathrm{d}z; \\
&\bar{\mathbf{D}}_{ums} = \int_{-h/2}^{h/2} \mathbf{C}_{ums} \left(1+f'\right) g \mathrm{d}z; \\
&\bar{\mathbf{D}}_{emb} = \int_{-h/2}^{h/2} \mathbf{C}_{emb} {g'}^2 \mathrm{d}z; \bar{\mathbf{D}}_{ems} = \int_{-h/2}^{h/2} \mathbf{C}_{ems} g^2 \mathrm{d}z; \\
&\bar{\mathbf{D}}_{eeb} = \int_{-h/2}^{h/2} \mathbf{C}_{eeb} {g'}^2 \mathrm{d}z; \bar{\mathbf{D}}_{ees} = \int_{-h/2}^{h/2} \mathbf{C}_{ees} g^2 \mathrm{d}z; \\
&\bar{\mathbf{D}}_{mmb} = \int_{-h/2}^{h/2} \mathbf{C}_{mmb} {g'}^2 \mathrm{d}z; \bar{\mathbf{D}}_{mms} = \int_{-h/2}^{h/2} \mathbf{C}_{mms} g^2 \mathrm{d}z
\end{aligned} \tag{21}$$

2.5. The isogeometric approximation

Employing the NURBS basic function [20], the displacement, electric and magnetic vectors are approximated as follows

$$\begin{aligned} \mathbf{u}(x,y) &= \sum_{I=1}^{m\times n} \mathbf{N}_I(x,y)\,\mathbf{q}_I; \\ \varphi(x,y) &= \sum_{I=1}^{m\times n} \mathbf{N}_{\varphi I}(x,y)\,\chi_I; \\ \psi(x,y) &= \sum_{I=1}^{m\times n} \mathbf{N}_{\psi I}(x,y)\,\chi_I \end{aligned} \tag{22}$$

where

$$\begin{aligned} \mathbf{N}_I(x,y) &= \begin{bmatrix} N_I(x,y) & 0 \\ 0 & N_I(x,y) \end{bmatrix}; \\ \mathbf{N}_{\varphi I}(x,y) &= \left\{ N_I(x,y) \quad 0 \right\}; \\ \mathbf{N}_{\psi I}(x,y) &= \left\{ 0 \quad N_I(x,y) \right\}; \\ \mathbf{q}_I &= \{w_{bI}, w_{sI}\}^T; \chi_I = \{\varphi_I, \psi_I\}^T \end{aligned} \tag{23}$$

where $\mathrm{N}_I(x,y)$ is the NURBS basic function.

By substituting Eq. (22) into Eq. (21), the strain, electric and magnetic fields can be re-expressed as

$$\begin{aligned} &\bar{\boldsymbol{\varepsilon}}^b = \sum_{I=1}^{m\times n} \begin{Bmatrix} \bar{\mathbf{B}}_{b1I} \\ \bar{\mathbf{B}}_{b2I} \end{Bmatrix} \boldsymbol{q}_I = \sum_{I=1}^{m\times n} \bar{\mathbf{B}}_I^b \boldsymbol{q}_I; \boldsymbol{\gamma}^s = \sum_{I=1}^{m\times n} \bar{\mathbf{B}}_I^s \mathbf{d}_I; \\ &\bar{\mathbf{E}}^b = \sum_{I=1}^{m\times n} \bar{\mathbf{B}}_{\varphi bI} \boldsymbol{\chi}_I; \bar{\mathbf{E}}^s = \sum_{I=1}^{m\times n} \bar{\mathbf{B}}_{\varphi sI} \boldsymbol{\chi}_I; \\ &\bar{\mathbf{H}}^b = \sum_{I=1}^{m\times n} \bar{\mathbf{B}}_{\psi bI} \boldsymbol{\chi}_I; \bar{\mathbf{H}}^s = \sum_{I=1}^{m\times n} \bar{\mathbf{B}}_{\psi sI} \boldsymbol{\chi}_I \end{aligned} \tag{24}$$

in which

$$\begin{aligned} &\boldsymbol{B}_{1I}^b = -\begin{bmatrix} N_{I,xx} & 0 \\ N_{I,yy} & 0 \\ 2N_{I,xy} & 0 \end{bmatrix}; \boldsymbol{B}_{2I}^b = \begin{bmatrix} 0 & N_{I,xx} \\ 0 & N_{I,yy} \\ 0 & 2N_{I,xy} \end{bmatrix}; \\ &\bar{\boldsymbol{B}}_I^s = \begin{bmatrix} 0 & N_{I,x} \\ 0 & N_{I,y} \end{bmatrix}; \bar{\mathbf{B}}_{\varphi bI} = \begin{bmatrix} 0 & 0 \\ 0 & 0 \\ -N_I & 0 \end{bmatrix}; \\ &\bar{\mathbf{B}}_{\psi bI} = \begin{bmatrix} 0 & 0 \\ 0 & 0 \\ 0 & -N_I \end{bmatrix}; \bar{\mathbf{B}}_{\varphi sI} = \begin{bmatrix} -N_{I,x} & 0 \\ -N_{I,y} & 0 \end{bmatrix}; \\ &\bar{\mathbf{B}}_{\psi sI} = \begin{bmatrix} 0 & -N_{I,x} \\ 0 & -N_{I,y} \end{bmatrix} \end{aligned} \tag{25}$$

Substituting Eq. (22) into Eq. (17), the vector N_w is reformed as

$$\boldsymbol{N}_w = \sum_{I=1}^{m\times n} \bar{\boldsymbol{B}}_{wI} \boldsymbol{q}_I;\ \bar{\mathbf{B}}_{wI} = \begin{bmatrix} N_{I,x} & N_{I,x} \\ N_{I,y} & N_{I,y} \end{bmatrix} \tag{26}$$

Substituting Eqs. (24) and (26) into Eq. (20), the weak form for buckling analysis of the MEE foam plate resting on a Winkler-Pasternak foundation can be presented as following

$$(\mathbf{K} - \lambda_{cr}\mathbf{K}_g)\,\mathbf{q} = 0 \tag{27}$$

where

$$\begin{aligned} &\mathbf{K} = \mathbf{K}_{uu} - \mathbf{K}_{u\chi}\mathbf{K}_{\chi\chi}^{-1}\mathbf{K}\mathbf{K}_{u\chi}^T; \mathbf{K}_g = \int_\Omega \mathbf{B}_w^T \mathbf{N}_m \mathbf{B}_w \mathrm{d}\Omega; \\ &\mathbf{K}_{uu} = \int_\Omega (\bar{\mathbf{B}}^b)^T \bar{\boldsymbol{D}}_{uu}^b \bar{\mathbf{B}}^b \mathrm{d}\Omega + \int_\Omega (\bar{\mathbf{B}}^s)^T \bar{\boldsymbol{D}}_{uu}^s \bar{\mathbf{B}}^s \mathrm{d}\Omega - \ldots \\ &\int_\Omega \mathbf{B}_w^T \mathbf{N}_{em} \mathbf{B}_w \mathrm{d}\Omega - \int_\Omega \mathbf{B}_w^T \left(k_w \mathbf{B}_w - k_s \nabla^2 \mathbf{B}_w\right) \mathrm{d}\Omega \\ &\mathbf{K}_{u\chi} = -\int_\Omega (\bar{\mathbf{B}}^b)^T \bar{\boldsymbol{D}}_{ueb} \bar{\mathbf{B}}_\varphi^b \mathrm{d}\Omega - \int_\Omega (\bar{\mathbf{B}}^s)^T \bar{\boldsymbol{D}}_{ues} \bar{\mathbf{B}}_\varphi^s \mathrm{d}\Omega - \ldots \\ &\int_\Omega (\bar{\mathbf{B}}^b)^T \bar{\boldsymbol{D}}_{umb} \bar{\mathbf{B}}_\psi^b \mathrm{d}\Omega - \int_\Omega (\bar{\mathbf{B}}^s)^T \bar{\boldsymbol{D}}_{ums} \bar{\mathbf{B}}_\psi^s \mathrm{d}\Omega; \\ &\mathbf{K}_{\chi\chi} = -\int_\Omega \bar{\mathbf{B}}_{\varphi b}^T \bar{\boldsymbol{D}}_{eeb} \bar{\mathbf{B}}_\varphi^b \mathrm{d}\Omega - \int_\Omega \bar{\mathbf{B}}_{\varphi s}^T \bar{\boldsymbol{D}}_{ees} \bar{\mathbf{B}}_\varphi^s \mathrm{d}\Omega - \ldots \\ &\int_\Omega \bar{\mathbf{B}}_{\varphi b}^T \bar{\boldsymbol{D}}_{emb} \bar{\mathbf{B}}_\psi^b \mathrm{d}\Omega - \int_\Omega \bar{\mathbf{B}}_{\varphi s}^T \bar{\boldsymbol{D}}_{ems} \bar{\mathbf{B}}_\psi^s \mathrm{d}\Omega - \ldots \\ &\int_\Omega \bar{\mathbf{B}}_{\psi b}^T \bar{\boldsymbol{D}}_{emb} \bar{\mathbf{B}}_\varphi^b \mathrm{d}\Omega - \int_\Omega \bar{\mathbf{B}}_{\psi s}^T \bar{\boldsymbol{D}}_{ems} \bar{\mathbf{B}}_\varphi^s \mathrm{d}\Omega - \ldots \\ &\int_\Omega \bar{\mathbf{B}}_{\varphi b}^T \bar{\boldsymbol{D}}_{mmb} \bar{\mathbf{B}}_\psi^b \mathrm{d}\Omega - \int_\Omega \bar{\mathbf{B}}_{\psi s}^T \bar{\boldsymbol{D}}_{mms} \bar{\mathbf{B}}_\psi^s \mathrm{d}\Omega \end{aligned} \tag{28}$$

in which λ_{cr} is critical buckling load, $\boldsymbol{K}_g$ is geometrical stiffness matrix.

3. Numerical Results

In order to validate the accuracy and consistency of the current method, we investigate the MEE FG plates with the material properties listed in Table 1 [35]. Table 2 presents the non-dimensional critical buckling load $\bar{N} = N_{cr}a^2/c_{11t}h^3$ of the fully simply supported (SSSS) MEE FG plates with even and uneven porous distributions under biaxial compressive load ($\mathrm{N}_x = \mathrm{N}_y = 1$) without an elastic foundation. We can see in Table 2, the numerical results obtained from the presented method are in good agreement with those provided by Ebrahimi [35]. The results of the comparison in

Table 2 demonstrate the precision and reliability of the present method.

Next, we consider the uniaxial mechanical buckling ($N_x = 1$, $N_y = 0$) of the rectangular MEE foam plate resting on the Winkler-Pasternak foundation with the material properties taken in Table 3. In addition, the nondimensional spring and shear coefficients of the Winkler-Pasternak foundation are normalized as follows

$$K_w = \frac{k_w c_{11} h^3}{a^4};\ K_s = \frac{k_s c_{11} h^3}{a^2} \qquad (29)$$

In addition, the boundary conditions (BCs) encompass a combination of clamped (C), simply supported (S), and free (F) edges. The dimensionless critical buckling load of the MEE foam plates resting on an elastic foundation is taken for the parametric study by

$$\hat{\bar{N}} = N_{cr} a^2 / c_{11} h^3 \qquad (30)$$

The effect of the porosity distribution and porous coefficient on the dimensionless critical buckling load of the MEE foam plate without an elastic foundation is presented in Table 4. We can see in Table 4 that a rise of the porosity coefficient leads to a decrease of the plate's stiffness, decreasing the critical buckling load of the MEE foam plate. Besides, the uniform porosity distribution provides the smallest critical buckling load, while the symmetric porosity distribution provides the largest. Table 5 and Table 6 tabulate the influence of initial external electric voltage and magnetic potential on the nondimensional critical buckling load of the MEE foam plate with various BCs. The results in Table 5 and Table 6 show that with a positive value of the external electric and magnetic potential, the critical buckling load of the MEE foam plate reduces and increases, respectively. Whereas the opposite response for critical buckling load with a negative value of the external electric and magnetic potentials. This is because the positive magnetic potential and negative electric voltage create the in-plane tensile force, which makes the plate stiffer. In contrast, the opposing magnetic and positive electric potential create the in-plane compressive force, reducing the plate stiffness. Next, the effect of the spring and shear coefficients and length-to-thickness ratio on the dimensionless buckling load of the MEE foam plates resting on an elastic foundation is shown in Table 7 and Table 8, respectively. As indicated by these tables, a rise in the spring and shear coefficients of the elastic foundation increases the plate's stiffness, producing in an increase of the critical buckling load. Additionally, the critical buckling load of the MEE foam plate increases as the length-to-thickness ratio increases. The dimensionless critical buckling load of the MEE foam plate resting on an elastic foundation with various width-to-length ratios is depicted in Figure 2. As demonstrated by Figure 2, a rise in the width-to-length ratio leads to a decrease in the critical buckling load. Finally, Figure 3 plots the first four buckling modes of the SSSS MEE foam square plate.

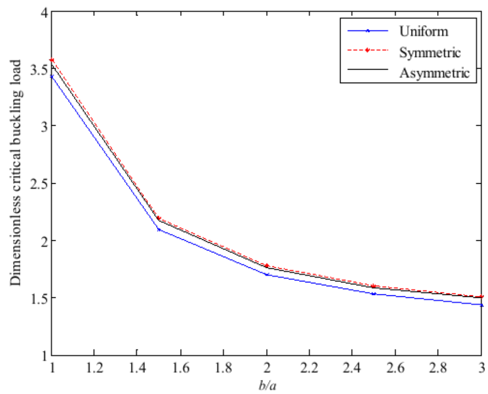

Fig. 2: Dimensionless critical buckling load of the SSSS MEE foam rectangular plates resting on elastic foundation with various width-to-length ratios ($a/h = 10$, $e_0 = 0.1$, $V_0 = \Omega_0 = 0$, $K_w = 1$, $K_s = 1$).

4. Conclusion

This article was presented the mechanical buckling of the MEE foam plates resting on a Winkler-Pasternak foundation according to the RPT with two variables and the IGA. The MEE foam plate comprises the MEE material with pores. The validity of the current method has been confirmed through comparisons with prior references. The effect of the porosity distributions, porous coefficient, initial external electric voltage and magnetic potential, foundation pa-

Tab. 1: The material properties of the MEE FG plates.

Properties	Top ($BaTi_2O_3$)	Bottom ($CoFe_2O_4$)
Elastic (GPa)	$c_{11} = c_{22} = 166$; $c_{33} = 162$; $c_{12} = 77$; $c_{13} = c_{23} = 78$; $c_{55} = 43$; $c_{66} = 44.5$	$c_{11} = c_{22} = 286$; $c_{33} = 269.5$; $c_{12} = 173$; $c_{13} = c_{23} = 170.5$; $c_{55} = 45.3$; $c_{66} = 56.5$
Piezoelectric (Cm^{-2})	$e_{31} = -4.4$; $e_{33} = 18.6$; $e_{15} = 11.6$	$e_{31} = 0$; $e_{33} = 0$; $e_{15} = 0$
Piezomagnetic (N/Am)	$q_{31} = q_{33} = q_{15} = 0$	$q_{31} = 580.3$; $q_{33} = 699.7$; $q_{15} = 550$
Dielectric (10^{-9} $C^2m^{-2}N^{-1}$)	$k_{11} = k_{22} = 11.2$; $k_{33} = 12.6$	$k_{11} = k_{22} = 0.08$; $k_{33} = 0.093$
Magnetic (10^{-6} Ns^2/C^2)	$\mu_{11} = \mu_{22} = 5$; $\mu_{33} = 10$	$\mu_{11} = \mu_{22} = -590$; $\mu_{33} = 157$
Magnetoelectric (10^{-12} Ns/VC)	$d_{11} = d_{22} = d_{33} = 0$	$d_{11} = d_{22} = d_{33} = 0$
Density (kg/m^3)	$\rho = 5800$	$\rho = 5300$

Tab. 2: The dimensionless critical buckling load of the MEE FG plate with various external electric voltage and porous volume fraction (p =2, a/h = 100, Ω0 = 0).

Type	V_0(V)	α					
		0		0.1		0.2	
		Ref. [35]	Present	Ref. [35]	Present	Ref. [35]	Present
Even porosity	-500	0.92876	0.9334	0.82967	0.8352	0.72971	0.7363
	-250	0.91233	0.9170	0.81467	0.8202	0.71618	0.7228
	0	0.89590	0.9006	0.79968	0.8052	0.70266	0.7093
	250	0.87948	0.8841	0.78468	0.7902	0.689135	0.6957
	500	0.86305	0.8677	0.76969	0.7752	0.67561	0.6822
Uneven porosity	-500	0.928761	0.9334	0.903227	0.9082	0.877596	0.8829
	-250	0.912334	0.9170	0.8875	0.8925	0.862577	0.8679
	0	0.895907	0.9006	0.871774	0.8767	0.847558	0.8529
	250	0.87948	0.8841	0.856047	0.8610	0.832539	0.8378
	500	0.863052	0.8677	0.840321	0.8453	0.81752	0.8228

Tab. 3: The material properties of the MEE foam plates.

Properties	$BaTi_2O_3$-$CoFe_2O_4$
Elastic (GPa)	$c_{11} = c_{22} = 226$; $c_{12} = 125$; $c_{13} = 124$; $c_{44} = c_{55} = 44.2$; $c_{66} = 50.5$
Piezoelectric (Cm^{-2})	$e_{31} = -2.2$; $e_{33} = 9.3$; $e_{15} = 5.8$
Piezomagnetic (N/Am)	$q_{15} = 275$; $q_{31} = q_{32} = 290.1$; $q_{33} = 349.9$
Dielectric (10^{-9} $C^2m^{-2}N^{-1}$)	$k_{11} = k_{22} = 5.64$; $k_{33} = 6.35$
Magnetic (10^{-6} Ns^2/C^2)	$\mu_{11} = \mu_{22} = -297$; $\mu_{33} = 83.5$
Magnetoelectric (10^{-12} Ns/VC)	$d_{11} = d_{22} = 5.367$; $d_{33} = 2737.5$
Density (kg/m^3)	$\rho = 5550$

Tab. 4: The effect of the porous distribution and porous coefficient on the critical buckling load of the MEE foam square plate (a/h = 10, $V_0 = \Omega_0 = 0$, $K_w = K_s = 0$).

Type	BCs	e_0			
		0.1	0.3	0.5	0.7
Uniform	SSSS	2.0821	1.7864	1.4727	1.1283
	SFSF	0.9735	0.8353	0.6886	0.5275
	SCSC	3.2816	2.8155	2.3211	1.7782
	CCCC	4.5740	3.9244	3.2352	2.4785
	CFCF	1.7457	1.4978	1.2348	0.9460
Symmetric	SSSS	2.1381	1.9616	1.7799	1.5866
	SFSF	1.0010	0.9210	0.8395	0.7501
	SCSC	3.3596	3.0577	2.7408	2.3910
	CCCC	4.6688	4.2155	3.7325	3.1882
	CFCF	1.7903	1.6367	1.4777	1.3050
Asymmetric	SSSS	2.0946	1.8334	1.5721	1.3104
	SFSF	0.9795	0.8582	0.7363	0.6145
	SCSC	3.2993	2.8836	2.4674	2.0501
	CCCC	4.5960	4.0110	3.4249	2.8369
	CFCF	1.7557	1.5358	1.3157	1.0951

Tab. 5: The dimensionless critical buckling load of the MEE foam square plate with various initial external electric voltages (a/h = 50, e_0 = 0.2, $\Omega_0 = 0$, $K_w = K_s = 0$).

Type	BCs	V_0 (V)				
		-500	-250	0	250	500
Uniform	SSSS	2.0691	2.0654	2.0618	2.0582	2.0545
	SFSF	0.9477	0.9447	0.9417	0.9387	0.9357
	SCSC	3.4724	3.4692	3.4661	3.4629	3.4598
	CCCC	5.1695	5.1662	5.1630	5.1598	5.1565
	CFCF	1.7857	1.7835	1.7814	1.7792	1.7770
Symmetric	SSSS	2.2048	2.2012	2.1975	2.1939	2.1903
	SFSF	1.0098	1.0068	1.0038	1.0008	0.9978
	SCSC	3.6995	3.6963	3.6931	3.6900	3.6868
	CCCC	5.5060	5.5027	5.4995	5.4962	5.4930
	CFCF	1.9027	1.9005	1.8984	1.8962	1.8940
Asymmetric	SSSS	2.1014	2.0978	2.0942	2.0905	2.0869
	SFSF	0.9625	0.9595	0.9565	0.9535	0.9505
	SCSC	3.5266	3.5234	3.5203	3.5171	3.5140
	CCCC	5.2499	5.2467	5.2434	5.2402	5.2369
	CFCF	1.8136	1.8114	1.8093	1.8071	1.8049

rameters and the parameters of the geometries on the critical buckling load of the MEE foam plates resting on a Winkler-Pasternak foundation has been examined. The numerical results show that the stiffness of the MEE foam plates reduces with a rise of the porous coefficient. The increase of the external magnetic potential leads to the growth of the plate's stiffness, while a rise of the external electric voltage decreases the plate's stiffness. Besides, the MEE foam plates become stiffer with a rise of the spring and shear coefficients of an elastic foundation. As the width-to-length and length-to-thickness ratios increase, the critical buckling load of the

Tab. 6: The dimensionless critical buckling load of the MEE foam square plate with various initial external magnetic potentials (a/h = 50, e_0 = 0.2, V_0 = 0, K_w = K_s = 0).

Type	BCs	Ω_0 (A)				
		-500	-250	0	250	500
Uniform	SSSS	1.9759	2.0189	2.0618	2.1047	2.1477
	SFSF	0.8706	0.9062	0.9417	0.9772	1.0125
	SCSC	3.3915	3.4288	3.4661	3.5033	3.5405
	CCCC	5.0860	5.1245	5.1630	5.2014	5.2398
	CFCF	1.7295	1.7554	1.7814	1.8073	1.8332
Symmetric	SSSS	2.1114	2.1545	2.1975	2.2406	2.2837
	SFSF	0.9325	0.9682	1.0038	1.0394	1.0749
	SCSC	3.6184	3.6558	3.6931	3.7305	3.7678
	CCCC	5.4223	5.4609	5.4995	5.5380	5.5765
	CFCF	1.8463	1.8723	1.8984	1.9243	1.9503
Asymmetric	SSSS	2.0080	2.0511	2.0942	2.1372	2.1803
	SFSF	0.8852	0.9209	0.9565	0.9921	1.0276
	SCSC	3.4455	3.4829	3.5203	3.5576	3.5950
	CCCC	5.1662	5.2048	5.2434	5.2820	5.3205
	CFCF	1.7572	1.7832	1.8093	1.8352	1.8612

Tab. 7: The influence of nondimensional spring coefficient Kw and length-to-thickness ratio on the dimensionless critical buckling load of the MEE foam square plate with uniform porous distribution resting on an elastic foundation (e_0 = 0.2, V_0 = Ω_0 = 0, K_s = 0).

K_w	BCs	a/h				
		10	20	30	40	50
1	SSSS	1.9965	2.0933	2.1123	2.1190	2.1222
	SFSF	0.9433	0.9724	0.9780	0.9799	0.9808
	SCSC	3.0932	3.4109	3.4759	3.4994	3.5104
	CCCC	4.2867	4.9756	5.1234	5.1771	5.2024
	CFCF	1.6336	1.7550	1.7790	1.7878	1.7919
2	SSSS	2.0569	2.1537	2.1726	2.1794	2.1826
	SFSF	0.9807	1.0106	1.0164	1.0184	1.0194
	SCSC	3.1348	3.4546	3.5199	3.5435	3.5546
	CCCC	4.3199	5.0136	5.1621	5.2162	5.2416
	CFCF	1.6438	1.7654	1.7895	1.7983	1.8024
3	SSSS	2.1173	2.2141	2.2330	2.2398	2.2430
	SFSF	1.0172	1.0482	1.0542	1.0563	1.0573
	SCSC	3.1761	3.4981	3.5638	3.5876	3.5987
	CCCC	4.3526	5.0513	5.2007	5.2551	5.2806
	CFCF	1.6540	1.7758	1.7999	1.8087	1.8129

MEE foam plate decreases and increases, respectively. Finally, the symmetric distribution yields the highest critical buckling load among the various porosity distributions. The uniform distribution results in the lowest critical buckling load for the MEE foam plates.

Tab. 8: The influence of nondimensional shear coefficient Ks and length-to-thickness ratio on the dimensionless critical buckling load of the MEE foam square plate with uniform porous distribution resting on an elastic foundation ($e_0 = 0.2$, $V_0 = \Omega_0 = 0$, $K_w = 0$).

K_s	BCs	a/h				
		10	20	30	40	50
1	SSSS	3.1282	3.2250	3.2439	3.2507	3.2539
	SFSF	1.8432	1.8845	1.8923	1.8951	1.8964
	SCSC	4.0492	4.3895	4.4582	4.4830	4.4946
	CCCC	5.2112	5.9693	6.1297	6.1880	6.2153
	CFCF	2.3349	2.4599	2.4847	2.4937	2.4980
2	SSSS	4.2531	4.4171	4.4360	4.4428	4.4459
	SFSF	2.5970	2.6650	2.6782	2.6829	2.6852
	SCSC	5.0197	5.3971	5.4718	5.4986	5.5112
	CCCC	5.9808	6.9634	7.1414	7.2058	7.2360
	CFCF	3.0404	3.1702	3.1958	3.2052	3.2096
3	SSSS	4.9981	5.3339	5.4057	5.4317	5.4439
	SFSF	3.2972	3.3682	3.3819	3.3869	3.3892
	SCSC	5.9587	6.3880	6.4708	6.5004	6.5143
	CCCC	6.7039	7.7457	7.9932	8.0852	8.1287
	CFCF	3.7408	3.8762	3.9029	3.9127	3.9173

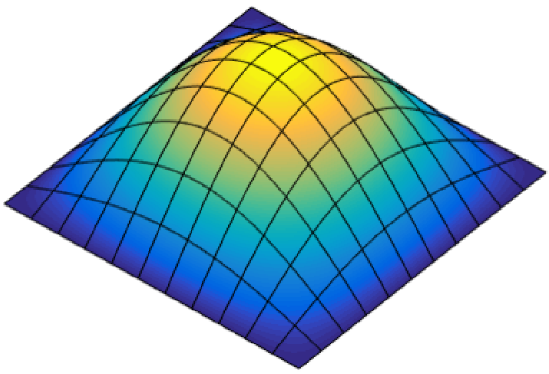

(a) Mode 1.

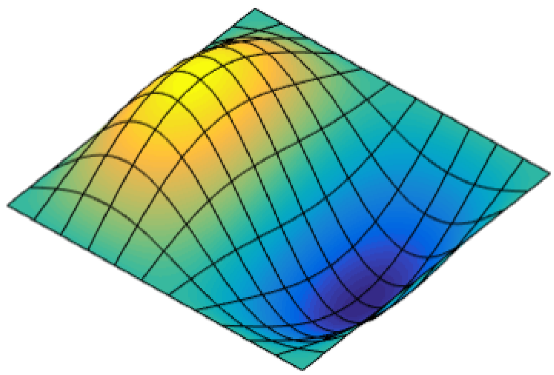

(b) Mode 2.

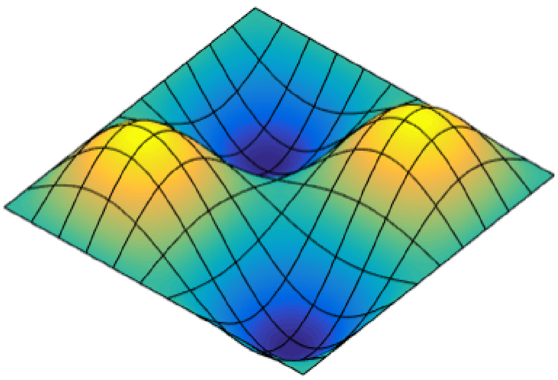

(c) Mode 3.

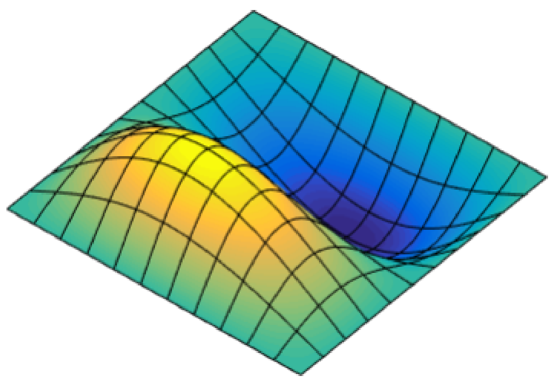

(d) Mode 4.

Fig. 3: The first four buckling modes of the SSSS MEE foam square plate.

References

[1] Ramirez, F., Heyliger, P.R., & Pan, E. (2006). Free vibration response of two-dimensional magneto-electro-elastic laminated plates. *Journal of Sound and Vibration*, *292*(3-5), 626–644.

[2] Xin, L. & Hu, Z. (2015). Free vibration of simply supported and multilayered magneto-electro-elastic plates. *Composite structures*, *121*, 344–350.

[3] Xin, L.b. & Hu, Z.d. (2012). Free vibration of fixed supported and multilayered magneto-electro-elastic plates. In *2012 Symposium on Piezoelectricity, Acoustic Waves, and Device Applications (SPAWDA)*, IEEE, 233–236.

[4] Li, Y. & Zhang, J. (2013). Free vibration analysis of magnetoelectroelastic plate resting on a Pasternak foundation. *Smart materials and structures*, *23*(2), 025002.

[5] Ebrahimi, F. & Barati, M. (2017). Buckling analysis of smart size-dependent higher order magneto-electro-thermo-elastic functionally graded nanosize beams. *Journal of Mechanics*, *33*(1), 23–33.

[6] Liu, M.F. (2016). Exact solution for the bending deformations of layered magneto-electro-elastic laminates based on thin-plate formulation. *International Journal of Engineering and Applied Sciences*, *3*(4), 257692.

[7] Jamalpoor, A., Ahmadi-Savadkoohi, A., & Hosseini-Hashemi, S. (2016). Free vibration and biaxial buckling analysis of magneto-electro-elastic microplate resting on visco-Pasternak substrate via modified strain gradient theory. *Smart Materials and Structures*, *25*(10), 105035.

[8] Ansari, R. & Gholami, R. (2017). Size-dependent buckling and postbuckling analyses of first-order shear deformable magneto-electro-thermo elastic nanoplates based on the nonlocal elasticity theory. *International Journal of Structural Stability and Dynamics*, *17*(01), 1750014.

[9] Shooshtari, A. & Razavi, S. (2016). Vibration analysis of a magnetoelectroelastic rectangular plate based on a higher-order shear deformation theory. *Latin American Journal of Solids and Structures*, *13*, 554–572.

[10] Razavi, S. (2017). On the Buckling the Behavior of a Multiphase Smart Plate based on a Higher-order Theory. *Mechanics of Advanced Composite Structures*, *4*(1), 47–58.

[11] Park, W.T. & Han, S.C. (2018). Buckling analysis of nano-scale magneto-electro-elastic plates using the nonlocal elasticity theory. *Advances in Mechanical Engineering*, *10*(8), 1687814018793335.

[12] Malikan, M., Nguyen, V.B., & Tornabene, F. (2018). Electromagnetic forced vibrations of composite nanoplates using nonlocal strain gradient theory. *Materials Research Express*, *5*(7), 075031.

[13] Wang, F., Zheng, Y.f., & Chen, C.p. (2018). Nonlinear bending of rectangular magnetoelectroelastic thin plates with linearly varying thickness. *International Journal of Nonlinear Sciences and Numerical Simulation*, *19*(3-4), 351–356.

[14] Yang, Y. & Li, X.F. (2019). Bending and free vibration of a circular magnetoelectroelastic plate with surface effects. *International Journal of Mechanical Sciences*, *157*, 858–871.

[15] Arefi, M. & Amabili, M. (2021). A comprehensive electro-magneto-elastic buckling and bending analyses of three-layered doubly curved nanoshell, based on nonlocal three-dimensional theory. *Composite Structures*, *257*, 113100.

[16] Hong, C.C. (2021). Vibration frequency of thick functionally graded material cylindrical shells with fully homogeneous equation and third-order shear deformation theory under thermal environment. *Journal of Vibration and Control*, *27*(17-18), 2004–2017.

[17] Sobhy, M. & Al Mukahal, F. (2022). Analysis of electromagnetic effects on vibration of

functionally graded GPLs reinforced piezo-electromagnetic plates on an elastic substrate. *Crystals*, *12*(4), 487.

[18] Kiran, M. & Kattimani, S. (2017). Buckling characteristics and static studies of multilayered magneto-electro-elastic plate. *Structural Engineering and Mechanics*, *64*(6), 751–763.

[19] Kiran, M. & Kattimani, S. (2018). Buckling analysis of skew magneto-electro-elastic plates under in-plane loading. *Journal of Intelligent Material Systems and Structures*, *29*(10), 2206–2222.

[20] Hughes, T.J., Cottrell, J.A., & Bazilevs, Y. (2005). Isogeometric analysis: CAD, finite elements, NURBS, exact geometry and mesh refinement. *Computer methods in applied mechanics and engineering*, *194*(39-41), 4135–4195.

[21] Bazilevs, Y., Takizawa, K., Tezduyar, T.E., Hsu, M.C., Otoguro, Y., Mochizuki, H., & Wu, M.C. (2020). Wind Turbine and Turbomachinery Computational Analysis with the ALE and Space-Time Variational Multiscale Methods and Isogeometric Discretization. *Journal of Advanced Engineering and Computation*, *4*(1), 1–32.

[22] Thai, C.H., Ferreira, A., & Nguyen-Xuan, H. (2018). Isogeometric analysis of size-dependent isotropic and sandwich functionally graded microplates based on modified strain gradient elasticity theory. *Composite Structures*, *192*, 274–288.

[23] Thai, C.H., Ferreira, A., & Phung-Van, P. (2019). Size dependent free vibration analysis of multilayer functionally graded GPLRC microplates based on modified strain gradient theory. *Composites Part B: Engineering*, *169*, 174–188.

[24] Thai, C.H., Ferreira, A., Rabczuk, T., & Nguyen-Xuan, H. (2018). Size-dependent analysis of FG-CNTRC microplates based on modified strain gradient elasticity theory. *European Journal of Mechanics-A/Solids*, *72*, 521–538.

[25] Tan, P., Nguyen-Thanh, N., & Zhou, K. (2017). Extended isogeometric analysis based on Bézier extraction for an FGM plate by using the two-variable refined plate theory. *Theoretical and Applied Fracture Mechanics*, *89*, 127–138.

[26] Huang, J., Nguyen-Thanh, N., & Zhou, K. (2017). Extended isogeometric analysis based on Bézier extraction for the buckling analysis of Mindlin–Reissner plates. *Acta Mechanica*, *228*, 3077–3093.

[27] Takizawa, K., Bazilevs, Y., Tezduyar, T.E., Hsu, M.C., & Terahara, T. (2022). Computational cardiovascular medicine with isogeometric analysis. *Journal of Advanced Engineering and Computation*, *6*(3), 167–199.

[28] Huang, J., Nguyen-Thanh, N., Gao, J., Fan, Z., & Zhou, K. (2022). Static, free vibration, and buckling analyses of laminated composite plates via an isogeometric meshfree collocation approach. *Composite Structures*, *285*, 115011.

[29] Zhang, Y., Ren, H., & Rabczuk, T. (2022). Nonlocal Operator Method for Solving Partial Differential Equations: State-of-the-Art Review and Future Perspectives. *J Adv Eng Comput*, *6*(1), 1.

[30] Zhou, L., Lin, X.h., Zhao, H.y., & Chen, J. (2017). Optimal multi-degree reduction of C-Bézier surfaces with constraints. *Frontiers of Information Technology & Electronic Engineering*, *18*(12), 2009–2016.

[31] Kiran, R., Nguyen-Thanh, N., Huang, J., & Zhou, K. (2021). Buckling analysis of cracked orthotropic 3D plates and shells via an isogeometric-reproducing kernel particle method. *Theoretical and Applied Fracture Mechanics*, *114*, 102993.

[32] Barati, M.R. (2017). Nonlocal-strain gradient forced vibration analysis of metal foam nanoplates with uniform and graded porosities. *Advances in nano research*, *5*(4), 393.

[33] Shimpi, R.P. (2002). Refined plate theory and its variants. *AIAA journal*, *40*(1), 137–146.

[34] Ke, L.L. & Wang, Y.S. (2014). Free vibration of size-dependent magneto-electro-elastic nanobeams based on the nonlocal theory. *Physica E: Low-Dimensional Systems and Nanostructures*, *63*, 52–61.

[35] Ebrahimi, F. & Jafari, A. (2016). Buckling behavior of smart MEE-FG porous plate with various boundary conditions based on refined theory. *Advances in materials Research*, *5*(4), 279.

About Authors

P. T. HUNG was born in Vietnam in 1981. He has a Ph.D. degree in Mechanics. Now, he is a lecturer at the Faculty of Civil Engineering at Ho Chi Minh City University of Technology and Education, Ho Chi Minh City, Vietnam. His research interests are the computational mechanics.

P. PHUNG-VAN received his Ph.D from Ghent University in 2016. He has been conducting computational mechanics research since 2012. Currently, he is a senior lecturer at the Faculty of Civil Engineering, HUTECH University, Ho Chi Minh City, Vietnam. He has published over 58 Web-of-Science-indexed journal articles on computational and structural mechanics and nanostructures. He is one of World's Best Mechanical and Aerospace Engineering Scientists according to Research.com.

